

Optimizing Air-borne Network-in-a-box Deployment for Efficient Remote Coverage

Sidrah Javed, *Member, IEEE*, Yunfei Chen, *Senior Member, IEEE*,
Mohamed-Slim Alouini, *Fellow, IEEE*, and Cheng-Xiang Wang, *Fellow, IEEE*

Abstract—Among many envisaged drivers for sixth generation (6G), one is from the United Nation’s Sustainability Development Goals 2030 to eliminate digital inequality. Remote coverage in sparsely populated areas, difficult terrains or emergency scenarios requires on-demand access and flexible deployment with minimal capex and opex. In this context, network-in-a-box (NIB) is an exciting solution which packs the whole wireless network into a single portable and re-configurable box to support multiple access technologies such as WiFi/2G/3G/4G/5G etc. In this paper, we propose low-altitude platform station (LAPS) based NIBs with stratospheric high-altitude platform station high-altitude platform station (HAPS) as backhaul. Specifically, backhaul employs non-orthogonal multiple access (NOMA) with superposition coding at the transmitting HAPS and successive interference cancellation (SIC) at the receiving NIBs, whereas the access link (AL) employs superposition coding along with the regularized zero-forcing (RZF) precoding at the NIB in order to elevate the computational overhead from the ground users. The required number of airborne NIBs to serve a desired coverage area, their optimal placement, user association, beam optimization, and resource allocation are optimized by maximizing the sum-rate of the AL while maintaining the quality of service. Our findings reveal the significance of thorough system planning and communication parameters optimization for enhanced system performance and best coverage under limited resources.

Index Terms—HAPS, non-orthogonal multiple access, network-in-a-box, unmanned aerial vehicles, and 6G.

I. INTRODUCTION

The upcoming generations of wireless communications envision a comprehensive network capable of delivering ubiquitous and resilient connections to eliminate the digital divide [1]–[3]. The emerging technologies, such as aerial communications, have the potential to reach the unconnected people in remote areas. These platforms, such as drones, balloons, aircrafts, and airships, offer unique advantages that can overcome limitations of traditional terrestrial and satellite communications [4], [5]. For instance, aerial platforms offer flexible deployment rendering rapid on-demand coverage with mobility in remote or disaster-affected areas [6], [7]. Moreover, they are promising candidates for extensive coverage to reach communities in geographically challenging locations. In addition, they may be less susceptible to disruption caused by natural disasters compared with ground-based infrastructure. These features make aerial communications a valuable tool for connecting unserved or underserved populations. They

can function synergistically with the existing ground and space infrastructure [8], thereby bridging the digital divide and connecting the unconnected.

In aerial communications, multiple platforms can be combined in multi-layer, where LAPS can offer access link (AL) to the ground user (GU)s whereas HAPS provides the backhaul links to all the serving LAPS. HAPS can be implemented in the form of airship, aircraft or tethered balloons, while, LAPS can be realized as unmanned aerial vehicle (UAV)s. Although HAPS are capable of directly connecting to the GUs using 4G LTE or 5G NR [9], but, the spectrum compatible with the existing GU equipment offers low throughput. On the other hand, employing LAPS as an intermediate layer between HAPS and GUs can increase the overall system throughput by allowing the use of higher frequency bands for backhaul and higher area throughput of LAPS.

The communication networks for aerial platforms must be adaptive and seamlessly integrable. In this context, NIB (portable network or pop-out network) emerges as a complete hardware and software solution in a compact reconfigurable package to provide on-demand access while supporting multiple radio access technology (RAT)s. With efficient size, weight, and power (SWaP) characteristics, NIBs can become the building blocks for generating flexible and adaptable networks [10]. NIBs render widespread applications in commercial, government, and private sectors for remote coverage, disaster relief or enhanced cyber security [11], [12]. The concept of a small portable network with few physical devices was conceived in the preliminary works in [13] and [14]. NIBs can either operate as a stand-alone network or co-exist with an exiting network. In this regard, Huang et al. [15] proposed a physical device that connects to the pre-existent base stations in order to restore the original mobile network. The stand-alone NIB-based network was investigated to support smart health IoT services and broadband services in rural areas [16]. Recently, an efficient online service function chain deployment algorithm was proposed for dynamic network function virtualization in NIBs for industrial applications [17]. Likewise, 6G-enabled NIB’s channel characteristics were explored for the internet of connected vehicles to realize full-coverage, full-spectrum, and full applications [18]. Another industrial application was the secure decentralized spatial crowd-sourcing for 6G-enabled NIBs, which enabled the collection/transmission of security information on the blockchain using NIB, without depending on the third party [19]. Moreover, EmergeNet provided reliable and rapidly deployable small-scale cellular network for emergency and disaster scenariosx which was based on self-organizing network to enable autonomous

S. Javed and Y. Chen are with the Department of Engineering, University of Durham, DH1 3LE, England. E-mail: {sidrah.javed, yunfei.chen}@durham.ac.uk, M.S. Alouini is with CEMSE Division, King Abdulah University of Science and Technology (KAUST), Thuwal, Makkah Province, 23955-6900 Saudi Arabia. E-mail: slim.alouini@kaust.edu.sa, and C.-X. Wang is with the National Mobile Communications Research Laboratory, School of Information Science and Engineering, Southeast University, Nanjing 211189, China. E-mail: chxwang@seu.edu.cn.

decision-making for optimal network functioning [20]. NIBs were used for remote coverage and emergency deployment owing to their cost effective design and deployment [21].

None of the existing works has studied the deployment issue of NIB. However, this is important for its efficient operation. In this paper, we jointly address the NIB deployment, resource allocation, service provisioning, and backhauling challenges. In this context, multiple UAV-borne NIB (UAVB-NIB) hover over the area of interest where each UAVB-NIB is equipped with downward facing antenna arrays for communication with GUs and upward facing antenna for connection with the HAPs. Highly directional antenna at UAVB-NIBs is used for backhaul link so that it can direct beam to HAPS mitigating the free-space path losses (FSPL). For backhaul, HAPS employs NOMA to serve different UAVB-NIBs that share the same spectral and temporal resources. In addition, each UAVB-NIB employs RZF precoding for GUs accessing same RAT in its coverage area. A holistic approach and suitable algorithms to tackle the aforementioned challenges while guaranteeing user's QoS, fairness, energy, and spectral efficiency are proposed. This work presents a novel sequential algorithm that can solve the problems of deployment, user association (UA), beam optimization and resource allocation to maximize the system performance with limited power, spectrum and time resources. The main contributions of this work are:

- Deployment problem is solved using Geometric Disk Cover (GDC) algorithm which determines the minimum number of required UAVB-NIBs and their locations. Moreover, the UA problem is resolved using greedy algorithm with the objective to maximize the SINR. Each user is served by one and only one spot beam for user fairness (UF) and interference mitigation.
- After the UA, UAVB-NIBs location optimization is conducted to minimize beam-width/beam-radius to serve the associated users. The reduced beamwidth renders directive beam with high power density and antenna gain.
- For backhaul, HAPS employs phased antenna arrays and NOMA scheme to serve all the UAVB-NIBs in its coverage area [22]. The closed-form solution to the NOMA power allocation problem is presented.
- For AL, we employ successive convex approximation (SCA) to iteratively allocate power to different RAT users with the target to maximize the achievable sum rate under QoS constraints and backhaul limitations.
- The achievable data rate, energy efficiency (EE), spectral efficiency (SE) and UF of the proposed system are investigated to quantify the performance gains of the proposed algorithms over the existing ones.

The rest of the paper is organized as follows: Section II describes the detailed system model for the communication between HAPS to UAVB-NIBs and between UAVB-NIBs and the GUs. Section III details the propagation model and link budget to incorporate both small-scale and large-scale fading effects in the access and backhaul channel. Next, achievable sum rates for the access and backhaul links are determined in Section IV. Subsequently, Section V formulates and solves the optimization problem. Numerical results are

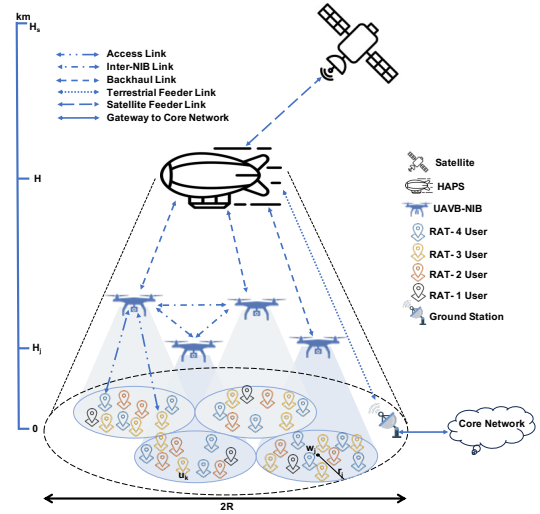


Fig. 1: NIB-based Aerial Communication System

illustrated in Section VI followed by the conclusions and acknowledgements in Section VII and VIII, respectively.

II. SYSTEM MODEL

In order to offer aerial coverage to a remote circular area of radius R having K GUs with coordinates $u_k \in \mathbb{R}^2 \forall k$ (on the horizontal plane), NIBs are mounted on UAVs for quick deployment. The coverage is offered by a fleet of J UAVB-NIBs, each hovering at an altitude H_j and covering a circular ground area with center w_j and 2D horizontal radius r_j where $j \in \{1, 2, \dots, J\}$, as shown in Fig 1. Each cell is served by a highly-directional and flexible beam from UAVB-NIB, using down-facing M antennas, allowing frequency reuse in the neighboring cells for efficient spectrum allocation and minimal interference. We employ software-defined network based NIB where each NIB j is capable of operating at various RATs $\Omega \in \{\text{WiFi}, 3\text{G}, 4\text{G}, 5\text{G}\}$ to serve K_j^Ω compatible users distributed uniformly in its coverage area. The number of users demanding RAT Ω follows the probability mass function Pr_Ω . We use the association parameters $\alpha_k^j \in \{0, 1\}$ and $\beta_k^\Omega \in \{0, 1\}$ to indicate that the user k is associated with j^{th} UAVB-NIB operating at RAT Ω , respectively, at a given time. We restrict $\sum_j \alpha_k^j = 1 \forall k$ for UF and $\sum_\Omega \beta_k^\Omega = 1 \forall k$ for effective resource allocation. The received signal at user k from j^{th} NIB operating at RAT Ω is given by:

$$y_{kj}^\Omega = \mathbf{h}_{kj}^{\Omega H} \mathbf{w}_{kj}^\Omega \alpha_k^j \beta_k^\Omega \sqrt{p_{kj}^\Omega P_j^\Omega s_{kj}^\Omega} + \sum_{\substack{l=1 \\ l \neq k}}^K \mathbf{h}_{kj}^{\Omega H} \mathbf{w}_{lj}^\Omega \alpha_l^j \beta_l^\Omega \sqrt{p_{lj}^\Omega P_j^\Omega s_{lj}^\Omega} + n_{kj}^\Omega, \quad (1)$$

where $\mathbf{h}_{kj}^\Omega \in \mathbb{C}^M$ is the channel vector between M antennas of j^{th} NIB and the single-antenna user k operating at RAT Ω , whereas $\mathbf{w}_{kj}^\Omega \in \mathbb{C}^M$ is the pre-coding vector for user k . Moreover, $p_{kj}^\Omega \in \mathbb{R}$ and $s_{kj}^\Omega \sim \mathcal{CN}(0, 1)$ are the allocated power coefficient and information bearing transmit signal for user k from NIB j on RAT Ω . Furthermore, P_j^Ω is the total transmission power budget of NIB j for RAT Ω . One has $\sum_k \alpha_k^j \beta_k^\Omega p_{kj}^\Omega = 1$ for all users in j^{th} cell using RAT Ω to ensure the expenses are within the available power budget. In

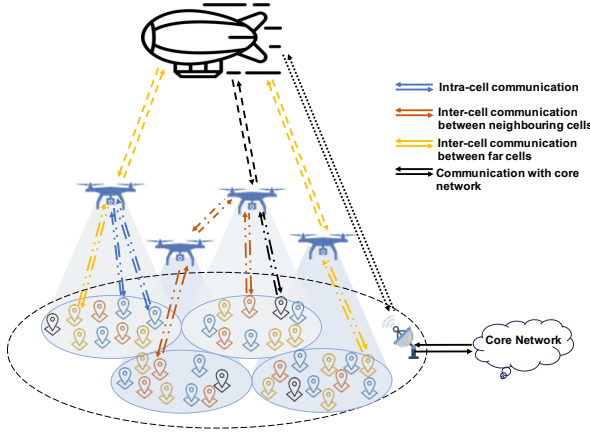


Fig. 2: Different Communication Scenarios

addition, the receiver thermal noise is modeled as a circular symmetric complex Gaussian random variable, i.e., $n_{kj}^\Omega \sim \mathcal{CN}(0, \sigma_{kj}^{\Omega 2})$. Let's define $\mathbf{H}_j^\Omega = [\mathbf{h}_{1j}^\Omega, \mathbf{h}_{2j}^\Omega, \dots, \mathbf{h}_{K_j j}^\Omega] \in \mathbb{C}^{M \times K_j}$ as the channel matrix comprising of channel coefficients between M transmit antennas of j^{th} UAVB-NIB operating at RAT Ω and the K_j associated users whereas $\mathbf{W}_j^\Omega = [\mathbf{w}_{1j}^\Omega, \mathbf{w}_{2j}^\Omega, \dots, \mathbf{w}_{K_j j}^\Omega] \in \mathbb{C}^{M \times K_j}$ being the precoding matrix for all connected users, such that the \mathbf{w}_{kj}^Ω intended for user k is orthogonal to every channel vector \mathbf{h}_{lj}^Ω associated with users $l \neq k$. Then, the received signal vector can be written as $\mathbf{y} = \mathbf{H}_j^{\Omega H} \mathbf{W}_j^\Omega \mathbf{x} + \mathbf{n}$, where \mathbf{x} and \mathbf{n} are the input signal vector and thermal noise vector at the receiver, respectively, with entries $\alpha_k^j \beta_k^\Omega \sqrt{p_{kj}^\Omega P_j^\Omega} s_{kj}^\Omega$ and n_{kj}^Ω for all associated users with j^{th} UAVB-NIB which are operating at RAT Ω . Therefore, the RZF pre-coder can be determined as [23]

$$\mathbf{W}_j^\Omega = \zeta_j^\Omega (\mathbf{H}_j^\Omega \mathbf{H}_j^{\Omega H} + \omega \mathbf{I}_M)^{-1} \mathbf{H}_j^\Omega, \quad (2)$$

where ω is the regularization scalar and ζ_j is the normalization scalar satisfying

$$\zeta_j^{\Omega 2} = \frac{1}{\text{tr}[(\mathbf{H}_j^\Omega \mathbf{H}_j^{\Omega H} + \omega \mathbf{I}_M)^{-1} \mathbf{H}_j^\Omega \mathbf{H}_j^{\Omega H} (\mathbf{H}_j^\Omega \mathbf{H}_j^{\Omega H} + \omega \mathbf{I}_M)^{-1}]}. \quad (3)$$

It is important to note that user k will only experience co-channel interference from users operating at the same RAT located within the same UAVB-NIB coverage area/cell. There is no inter-RAT interference as they operate at different frequency bands. Thus, the SINR γ_{kj}^Ω of the received signal y_{kj}^Ω can be derived as

$$\gamma_{kj}^\Omega = \frac{|\mathbf{h}_{kj}^{\Omega H} \mathbf{w}_{kj}^\Omega|^2 \alpha_k^j \beta_k^\Omega p_{kj}^\Omega}{\sum_{l=1, l \neq k}^{K_j} |\mathbf{h}_{kj}^{\Omega H} \mathbf{w}_{lj}^\Omega|^2 \alpha_l^j \beta_l^\Omega p_{lj}^\Omega + (\bar{\gamma}_{kj}^\Omega)^{-1}}, \quad (4)$$

where, $\bar{\gamma}_{kj}^\Omega = P_j^\Omega / \sigma_{kj}^{\Omega 2}$ is the transmit SNR with noise variance $\sigma_{kj}^{\Omega 2}$ (dBm) = $-174 + 10 \log(B_j^\Omega) + \text{NF}_k$. Here, B_j^Ω depicts the allocated channel bandwidth by j^{th} UAVB-NIB for RAT Ω and NF_k denotes the noise figure of the k^{th} user [24]. Fig. 2 illustrates different communication scenarios in the AL: Scenario I is the intra-cell communication within the UAVB-NIB coverage area, Scenario II is the inter-cell communication between GUs through the neighboring NIBs, Scenario

III is the inter-cell communication of GUs between distant UAVB-NIBs, and Scenario IV is the communication with core network. Interestingly, the NIB base stations are capable of independent routing and communicating in Scenarios I and II, whereas in Scenarios III and IV the communication is carried through the backhaul link.

For the backhaul, consider a typical unmanned solar-powered quasi-stationary HAPS at an altitude H over the desired coverage area with radius R ranging between 60km-400km. The HAPS operates from the stratospheric location (preferably between 18km-24km), pertaining to the suitable atmospheric conditions for the stable flight operation. HAPS provides backhaul links to J UAVB-NIBs over the fourth-generation (4G) long-term evolution (LTE) or 5G new radio (NR) air interfaces. It can further be connected to the terrestrial or satellite gateway through the RF feeder link [9] or free-space optical communication link [25]. HAPS communication panel employs phased antenna arrays to fixate the coverage relative to the station-keeping flight pattern. Within the coverage area, the channel gain varies by increasing the distance from the beam center. The strongest channel gain is available along the boresight direction $\theta = 0$. However, as the distance varies and/or the azimuth direction deviates from the boresight, the performance can be degraded due to the increased path loss and reduced antenna radiation pattern gain. The striking difference in the channel gains of the connected UAVB-NIBs enables us to reap maximum benefits offered by non-orthogonal multiple access (NOMA). Considering the DL-NOMA scenario, where the UAVB-NIBs are served by a directional beam with superposition coding as ¹

$$\bar{x} = \sum_{j=1}^J \sqrt{f_j P_H} x_j, \quad (5)$$

where P_H is the available power budget for transmission after deducting the aerodynamics, electronics, and night-time operational expenses from the available solar power at a given time [26]. Moreover, f_j and x_j are the fraction of power allocated to and intended information signal for the j^{th} UAVB-NIB, respectively. It is important to highlight that $\sum_{j=1}^J f_j \leq 1$ in order to limit the power division within given budget. Thus, using conventional wireless communication model, the received signal at j^{th} NIB from the HAPS is given by

$$v_j = g_j \sqrt{f_j P_H} x_j + g_j \sum_{\substack{i=1 \\ i \neq j}}^J \sqrt{f_i P_H} x_i + z_j, \quad (6)$$

where, g_j is the channel gain coefficient between the HAPS array panel and j^{th} UAVB-NIB and z_j is the receiver thermal noise modeled as circular symmetric complex Gaussian random variable, i.e., $z_j \sim \mathcal{CN}(0, \sigma_j^2)$. Clearly, the j^{th} NIB receives the superposed signal and retrieves its own signal using the ordered arrangement j_1, j_2, \dots, j_J depending on their increasing channel strengths. UAVB-NIB performs SIC by first decoding the information from NIB 1 to $j-1$ and then subtracting it from the received signal. Thus, it can decode its own signal from the resultant by considering the interference from $j+1$ to J as noise. Therefore, the signal-to-interference

¹The transmitted/received signals, channel gains and allocated powers are function of time. However, the time notation is omitted for brevity.

noise ratio Γ_j for the HAPS-NIB link at the j^{th} UAVB-NIB is given by

$$\Gamma_j = \frac{|g_j|^2 f_j P_H}{|g_j|^2 P_H \sum_{i=j+1}^J f_i + \sigma_j^2}, \quad (7)$$

whereas, the NIB with the strongest channel gain can successfully decode the information of all other UAVB-NIBs, rendering the SINR

$$\Gamma_J = \frac{|g_J|^2 f_J P_H}{\sigma_J^2}, \quad (8)$$

where the noise power is given as

$$\sigma_j^2 (\text{dBm}) = -174 + 10 \log(B_H) + \text{NF}_j, \quad (9)$$

with NF_j denoting the noise figure of the j^{th} NIB [24] and B_H depicting the HAPS channel bandwidth of the backhaul link. It is noteworthy that this work focuses on the downlink communications from HAPS to UAVB-NIBs and then from UAVB-NIBs to GUs. The uplink communication is reciprocal of the downlink communication, however, it will have an additional constraint to bound the transmit data-rate of the associated users according to the backhaul capacity limit, in order to avoid the delays at NIBs.

III. LINK BUDGET

In the aerial communication system, the radio signal propagation from aerial platform undergoes both small-scale and large-scale multipath fading. Moreover, the link channel gain is also dependent on the transmitter antenna gain and the receiver position. In this section, we will carry out link budgeting to model the propagation loss for both HAPS-NIB and NIB-GU links.

A. NIB-GU AL

The link between the UAVB-NIBs and GUs experiences FSPL and multipath fading due to the vertical distance between them and obstacles around the UE, respectively. Thus, each channel coefficient h_{kj}^Ω in the channel vector \mathbf{h}_{kj}^Ω can be expressed as:

$$|h_{kj}^\Omega|^2 = \frac{|\tilde{h}_{kj}^\Omega|^2 G_{jk}^\Omega}{L_{jk}^\Omega}, \quad (10)$$

where \tilde{h}_{kj}^Ω is the small-scale fading coefficient between the j^{th} UAVB-NIB and k^{th} user operating at RAT Ω . The AL is assumed to be non-LOS dominant and hence $|\tilde{h}_{kj}^\Omega|$ is modeled as a Rayleigh distribution with scale parameter \mathcal{U} having independently and identically normal distributed real and imaginary components i.e., $\Re\{\tilde{h}_{kj}^\Omega\} \sim \mathcal{N}(0, \mathcal{U}^2)$ and $\Im\{\tilde{h}_{kj}^\Omega\} \sim \mathcal{N}(0, \mathcal{U}^2)$. The probability density function of the Rayleigh distribution is well-known to be

$$f(x | \mathcal{U}) = \frac{x}{\mathcal{U}^2} \exp\left(-\frac{x^2}{\mathcal{U}^2}\right), \quad x \geq 0 \quad (11)$$

Moreover, UAVB-NIB employs antenna arrays so as to generate a single high-gain dynamic beam and the beam gain from the j^{th} NIB to user k is given by G_{jk}^Ω which is mainly determined by the off-axis angle between the GU and the main lobe direction of the UAVB-NIB beam [27]

$$G_{jk}^\Omega = G_{\max} \left(\frac{\mathcal{J}_1(\mu_{jk})}{2\mu_{jk}} + 36 \frac{\mathcal{J}_3(\mu_{jk})}{(\mu_{jk})^3} \right)^2, \quad (12)$$

where G_{\max} is the maximum beam gain along the boresight direction whereas \mathcal{J}_1 and \mathcal{J}_3 are the first-kind Bessel functions

of order 1 and 3, respectively, and

$$\mu_{jk} = \frac{2.07123 \sin \theta_{jk}}{\sin \theta_j^{3\text{dB}}}, \quad (13)$$

with $\theta_j^{3\text{dB}}$ representing the one-sided half-power beam width of j^{th} UAVB-NIB transmit antenna and θ_{jk} marking the offset angle of user k from the beam center. This allows on-demand dynamic beam as per the user distribution, which improves coverage efficiency. In addition, L_{jk}^Ω in (10) is the path loss as a function of the distance between j^{th} UAVB-NIB and k^{th} user operating at RAT Ω as [28]:

$$L_{jk}^\Omega [\text{dB}] = \frac{A}{1 + a \exp(-b(\phi_{jk} - a))} + B_{jk}^\Omega, \quad (14)$$

where

$$A = \eta_{\text{LOS}} - \eta_{\text{NLOS}}, \quad (15)$$

$$B_{jk}^\Omega = 20 \log_{10}(d_{jk}) + 20 \log_{10} \left(\frac{4\pi f_c^\Omega}{c} \right) + \eta_{\text{NLOS}}, \quad (16)$$

$$\phi_{jk} = \arcsin \left(\frac{H_j}{d_{jk}} \right), \quad (17)$$

with $\eta_{\text{LOS}}, \eta_{\text{NLOS}}, a,$ and b denoting the constant environment-related parameters while ϕ_{jk}, c, f_c^Ω and d_{jk} denote the elevation angle of user k from UAVB-NIB j , speed of light, carrier frequency of RAT Ω and distance between the user k and UAVB-NIB j . Consequently, the linear pathloss in (10) is $L_{jk}^\Omega = 10^{L_{jk}^\Omega [\text{dB}]/10}$.

B. HAPS-NIB Backhaul

The backhaul link also undergoes both small-scale fading \tilde{g}_j and large-scale fading L_j^{HAPS} . Hence, the channel coefficient g_j can be expressed as follows:

$$|g_j|^2 = \frac{|\tilde{g}_j|^2 G_j^{\text{HAPS}}}{L_j^{\text{HAPS}}}, \quad (18)$$

where $|\tilde{g}_j|$ is assumed to be Ricean distributed with LOS dominant characteristics between HAPS and UAVB-NIBs. Its probability distribution is given as the magnitude of a circularly-symmetric non-central bivariate normal random variable such as [30]–[32]

$$f(x | \nu, \sigma_f) = \frac{x}{\sigma_f^2} \exp\left(-\frac{(x^2 + \nu^2)}{2\sigma_f^2}\right) I_0\left(\frac{x\nu}{\sigma_f^2}\right), \quad (19)$$

where I_0 denotes the zeroth-order modified Bessel function of the first kind whose shape parameter K_s is defined by the ratio between the average power of LOS component and the average power associated with NLOS multipath components i.e., $K_s = \nu^2/2\sigma_f^2$. The transmitter antenna gain G_j^{HAPS} from HAPS to the j^{th} UAVB-NIB depends on the antenna aperture efficiency η , half-power beamwidth of the antenna $\theta_m^{3\text{dB}}$, HAPS altitude H , UAV altitude H_j and the distance of the UAVB-NIB j from the center of the HAPS beam w_0 with [33]

$$[G_j^{\text{HAPS}}]_{\text{dB}} = [G_0^{\text{HAPS}}]_{\text{dB}} - 12 \frac{G_0^{\text{HAPS}}}{\eta} \left(\frac{\theta_j}{70\pi} \right)^2, \quad (20)$$

where the peak HAPS antenna beam gain is $G_0^{\text{HAPS}} = \eta (70\pi/\theta_m^{3\text{dB}})^2$ and the beam angle (angle of departure) of the j^{th} UAVB-NIB can be derived using

$$\theta_j = \tan^{-1} \left(\frac{\|w_j - w_0\|}{H - H_j} \right). \quad (21)$$

²Note that the HAPS station-keeping flight does not contribute to the fast fading since there is no moving scatter surrounding the aircraft [29].

Evidently, the antenna directivity gain reduces while moving away from the boresight position in a horizontal plane. Finally, the L_j^{HAPS} is the FSPL as a function of the distance between HAPS and j^{th} UAVB-NIB i.e., d_j^m . We employ the space communication model for the aerial HAPS to compute the received signal path loss L_j^{HAPS} as [34]

$$L_j^{\text{HAPS}} = \frac{16\pi^2 d_j^2}{\lambda^2}, \quad (22)$$

where λ is the wavelength corresponding to the carrier frequency of HAPS. The FSPL renders the ratio between transmit power and received power.

IV. PERFORMANCE MEASURE

The overall performance of the system depends on the capacity of the AL as well as the backhaul link. We can evaluate the system performance in terms of achievable sum rate in the access and backhaul link.

We adopt a system where UAVB-NIB serves all RAT Ω users in its coverage area simultaneously. They all share the same bandwidth B_j^Ω and transmit with different power and precoding vectors to employ RZF precoding at the receiver for error-free detection. Considering linear precoding, the information rate for user u_{kj}^Ω is given by

$$R_{kj}^\Omega = B_j^\Omega \log_2(1 + \gamma_{kj}^\Omega). \quad (23)$$

Consequently, the sum rate of the AL is given by $R_a = \sum_{j=1}^J \sum_{k=1}^K \sum_{\Omega} R_{kj}^\Omega$ which aggregates the downlink data rate from all the UAVB-NIBs to the associated users operating at the desired RAT technologies. Thus,

$$R_a = \sum_{j=1}^J \sum_{\Omega} B_j^\Omega \sum_{k=1}^K \log_2(1 + \gamma_{kj}^\Omega). \quad (24)$$

On the other hand, the backhaul link employs DL-NOMA at the HAPS and each UAVB-NIB receives the superposed signal and performs SIC based on the channel strength ordering to decode its own signal. Assuming perfect receiver channel state information (CSI), we get accurate NIB-ordering and error-free decoding. Thus, the achievable rate of j^{th} UAVB-NIB is given by

$$R_j = B_H \log_2 [1 + \Gamma_j]. \quad (25)$$

conditioned on $R_{j \rightarrow l} > \tilde{R}_j \forall j \leq l$, where \tilde{R}_j is the target data rate of the j^{th} NIB while $R_{j \rightarrow l}$ denotes the rate of the l^{th} NIB to detect j^{th} NIB's message when $j \leq l$ in NIB ordering i.e.,

$$R_{j \rightarrow l} = B_H \log_2 \left(1 + \frac{|g_l|^2 f_j P_H}{|g_l|^2 P_H \sum_{i=j+1}^J f_i + \sigma_j^2} \right) \geq \tilde{R}_j. \quad (26)$$

Thus, the sum rate R_b of all UAVB-NIBs can be written as $R_b = \sum_{j=1}^J R_j$ yielding

$$R_b = \sum_{j=1}^J R_j = B_H \sum_{j=1}^J \log_2 [1 + \Gamma_j], \quad (27)$$

where the received SINR at j^{th} NIB in (7) can be expressed using (18) as

$$\Gamma_j = \frac{f_j}{\sum_{i=j+1}^J f_i + \aleph_j}, \quad (28)$$

where,

$$\aleph_j = \frac{\sigma_j^2 L_j^{\text{HAPS}}}{P_H |\tilde{g}_j|^2 G_j^{\text{HAPS}}}. \quad (29)$$

Likewise, the SINR of UAVB-NIB with the strongest channel gain Γ_J in (8) can be manifested using (18) as

$$\Gamma_J = f_J / \aleph_J. \quad (30)$$

V. PROBLEM FORMULATION AND SOLUTION

This work aims to jointly optimize the sum rate of all users in the coverage area of HAPS while guaranteeing their quality-of-service (QoS), UF, and expenses within the available power budget. This optimization problem is targeted at optimizing:

- 1) UAV deployment: J the number of UAVB-NIB to serve all users in the coverage area, the UAV locations \mathbf{w}_j (i.e., ground projection or center of coverage cells in 2D horizontal plane) and favorable hovering altitudes H_j of each UAVB-NIB.
- 2) UA: α_k^j the association variable between the users and the UAVB-NIBs for the given β_k^Ω i.e., the user demand for particular RAT Ω .
- 3) Beam optimization signifying the 3dB half-power beamwidths (HPBW) θ_j and beam-radii r_j of each participating UAVB-NIB.
- 4) NOMA power allocation factors f_j for each UAVB-NIB.
- 5) NIB power allocation factors p_{kj}^Ω for each user in its coverage area demanding a particular RAT service.

We formulate the design problem to maximize the sum data rate of all users in the access downlink communication in the heterogeneous communication system as:

$$\mathbf{P1} : \underset{\substack{J, \mathbf{w}_j, H_j, p_{kj}^\Omega, f_j, \\ \theta_j, r_j, \alpha_k^j \forall k, j}}{\text{maximize}} \sum_{j=1}^J \sum_{k=1}^K \sum_{\Omega} B_j^\Omega \log_2(1 + \gamma_{kj}^\Omega) \quad (31a)$$

$$\text{s.t.} \quad R_a(\gamma_{kj}^\Omega) \leq R_b(\Gamma_j), \quad \forall k \in K_1, j, \Omega \quad (31b)$$

$$R_{kj}^\Omega \geq R_{\min}, \quad \forall k, j, \Omega \quad (31c)$$

$$\alpha_k^j \in \{0, 1\} \& \sum_{j=1}^J \alpha_k^j = 1, \quad \forall k, j \quad (31d)$$

$$\sum_{j=1}^J \alpha_k^j \|\mathbf{u}_k - \mathbf{w}_j\| \leq \sum_{j=1}^J \alpha_k^j r_j, \quad \forall k \quad (31e)$$

$$\theta_{\min} \leq \theta_j^{\text{3dB}} \leq \theta_{\max}, \quad \forall j \quad (31f)$$

$$H_{\min} \leq H_j \leq H_{\max}, \quad \forall j \quad (31g)$$

$$R \geq r_j \geq 0.443 \lambda^\Omega H_j / D, \quad \forall j \quad (31h)$$

$$R_{j \rightarrow l} \geq \tilde{R}_j, \quad \forall j \leq l \quad (31i)$$

$$\sum_k \sum_{\Omega} \alpha_k^j \beta_k^\Omega p_{kj}^\Omega \leq 1, \quad \forall j \quad (31j)$$

$$0 \leq p_{kj}^\Omega \leq 1, \quad \forall k, j, \Omega \quad (31k)$$

$$\sum_j f_j \leq 1, \quad \forall j \quad (31l)$$

$$0 \leq f_j \leq 1, \quad \forall j \quad (31m)$$

$$f_1 \geq f_2 \geq \dots \geq f_J \quad (31n)$$

$$1 \leq J \leq K \quad (31o)$$

The constraint (31b) ensures that the sum rate of the GUs in the AL does not exceed the sum rate of the serving UAVB-NIBs in the backhaul link. The user set K_1 comprises of all users communicating in Scenarios III and IV in Fig. 2. The QoS rate constraint (31c) ensures that each GU is guaranteed the minimum rate threshold R_{\min} . The constraint (31d) restricts the Boolean entries $\alpha_k^j \in \{0, 1\}, \forall k, j$ (where $1 \leq k \leq K$

and $1 \leq j \leq J$) and the UA limits users to connect to any one UAVB-NIB at a given time for UF and effective utilization of the given resources. Moreover, the constraint (31e) ensures that the associating user resides within the beam coverage area of UAVB-NIB. The essential bounds on the 3dB HPBW, UAVB-NIB altitude, and beam radii, are guaranteed by the constraints (31f), (31g) and (31h), respectively. The spot beams of UAVB-NIB can be adjusted by the beamwidth control. It is worth noting that a narrower beam than the given bounds is not achievable with the given antenna array dimensions. In addition, the rate constraint (31i) warrants the successful information decoding of all NIBs with weaker channel gains at NIBs with strong channel conditions to avoid error propagation. Next, the constraints (31j) and (31k) limit the total transmission power and individual power factor of each GU within the available power budget. The sum of power coefficients of all users operating at Ω within the same NIB coverage cannot exceed 1. Likewise, the power limitations on NIB are given by (31l) and (31m). The optimal NIB power factor ordering in (31n) allocates more power to the weak users and vice versa for UF. Lastly, the bounds on the number of deployed UAVB-NIB are constrained (31o).

The problem **P1** is a non-convex mixed integer programming problem. Therefore, we divide this problem into sub-problems and solve these sub-problems sequentially and iteratively. The subproblems are solved for fewer optimization parameters assuming that other design parameters are fixed.

A. UAVB-NIB Deployment

The first challenge is to identify the number of UAVB-NIBs J to cover a remote area of radius R and user distribution K . Each NIB hovering at an altitude H_j offers the coverage to the ground circular area using high-density narrow spot beam with beamwidth $\theta_j^{3\text{dB}} \in \mathbb{R}$, beam radius $r_j \in \mathbb{R}^+$, and beam location³ $\mathbf{w}_j \in \mathbb{R}^2$ for all $j \in \{1, 2, \dots, J\}$ as detailed in Fig. 1. Interestingly, the variable J ranges between $1 \leq J \leq K$, reflecting that there can be at least one NIB to serve all GUs or a maximum of K UAVB-NIBs to individually serve each user. Both of these bounds are very loose. The lower bound is unrealistic for a large coverage area as the UAVB-NIB has a limited coverage whereas the upper bound is economically unsuitable. In essence, the value of J is a trade-off between SINR and efficient allocation of resources. The higher value of J renders highly directional beams with concentrated power, improved SINR and higher data rates but inefficient and uneconomical resource allocation. Therefore, we need to find the minimal number of UAVB-NIBs and their respective locations to cover all the users with a given user distribution. The UAVB-NIB altitude and coverage radius are related to each other through half-power beamwidth of the spot beam as:

$$r_j = H_j \tan \left(\frac{\theta_j^{3\text{dB}}}{2} \right). \quad (32)$$

Intuitively, for a given HPBW of NIB antennas, we can increase or decrease the UAV altitude to adjust the beam

³Beam location indicates the center of the beam with maximum antenna gain in the boresight direction

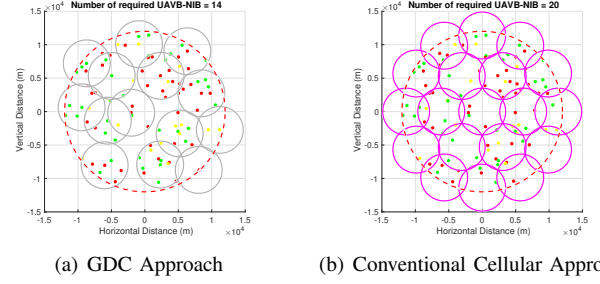


Fig. 3: Required number of UAVB-NIBs for user-connectivity in a given coverage area

radius for suitable coverage. Our findings reveal that R_a monotonically increases with J , but it is not economically feasible to deploy such a large number of UAVB-NIBs. The problem can have multiple solutions based on the economic constraints:

- Based on the relation $r_j = H_j \tan \theta_j$, we can use the lower bounds of the UAVB-NIB altitude and beam width to find the minimal possible beam radius.
- Find $r_j \forall j$ which satisfies the constrained inequality (31b) with equality i.e., $R_a = R_b$.

Problem **P1** can be decomposed as the sub-problem **P1(a)** for optimal UAVB-NIBs deployment given the beam coverage radius $r_j \forall j$;

$$\mathbf{P1(a)} : \underset{J, \mathbf{w}_j}{\text{minimize}} J \quad (33a)$$

$$\text{s.t.} \quad (31d), (31e), (31o) \quad (33b)$$

This sub-problem finds the optimal locations (beam centers w_m) of the minimal number of beams required to cover the users in the disk of radius R i.e., the coverage area of HAPS communication system. Problem **P1(a)** is a well-known geometric disk cover (GDC) problem which aims to find minimum number of disks of given radius to cover a set of points in the plane. The famous GDC problem is NP-hard highlighting the NP-hardness of **P1(a)**.

The problem can alternately be reformulated as the identification problem for a set of points:

$$\mathbf{P1(a1)} : \underset{\mathbf{z} \in \mathbb{B}^K}{\text{minimize}} \mathbf{1}^T \mathbf{z} \quad (34a)$$

$$\text{s.t.} \quad \mathbf{z}_k \in \{0, 1\}, \forall k \quad (34b)$$

$$\mathbf{Dz} \geq \mathbf{1} \quad (34c)$$

where \mathbf{D} is the symmetric boolean matrix with entries

$$d_{kl} = \begin{cases} 1, & \|\mathbf{u}_k - \mathbf{u}_l\|_2 \leq r_j, \\ 0, & \text{otherwise.} \end{cases} \quad (35)$$

To summarize, this problem identifies the minimum possible set of points from all the user coordinates such that if we draw the circles of radius r_j around these points then it will encompass all the points in its surrounding. We mark this set of points as the UAVB-NIB central positions and $\sum z^* = J^*$. This is a linear programming problem which can be easily solved using Lagrange function and KKT conditions for lower dimensions. The *intlinprog* package in MATLAB can efficiently yield the UAVB-NIB deployment parameters for higher dimensional problems. Fig. 3 illustrates an example

of optimal deployment strategy for the coverage to a given set of users. GDC approach requires 14 UAVB-NIBs in Fig. 3(a) as opposed to the 20 required UAVB-NIBs in Fig. 3(a) with conventional cellular approach.

B. Association Parameter

We assume that all NIBs are capable of operating at all RATs depending on the demands from the associated users. In this context, any user can connect to any UAVB-NIB. However, for UF and higher system efficiency, each user is allowed to associate with one and only one UAVB-NIB. Intuitively, the sum rate is maximized when the SINR γ_{kj}^Ω is maximized (for a given bandwidth for Ω RAT) owing to the monotonically increasing nature of logarithmic functions for $\gamma_{kj}^\Omega > 0$. Hence, the UA problem aims at finding the association parameters $\alpha_k^j, \forall k, j$ can be restructured as subproblem **P1(b)**:

$$\begin{aligned} \mathbf{P1(b)} : \text{maximize} \quad & \sum_{j=1}^J \sum_{k=1}^K \sum_{\Omega} \gamma_{kj}^\Omega (\alpha_{kj}^\Omega) \quad (36a) \\ \text{s.t.} \quad & (31d) \text{ and } (31e). \quad (36b) \end{aligned}$$

Constraint (31e) ensures that all the associated users of UAVB-NIB reside within its coverage area inside the main lobe of the antenna beam to be served simultaneously [35]. However, it is noteworthy that a user k may reside within the radius of UAVB-NIB j while being associated with another UAVB-NIB j' in overlapping coverage zones. The solution to this association parameter problem can be quantified using the greedy algorithm as:

$$\alpha_k^j = \begin{cases} 1, & \gamma_k^j \geq \gamma_k^{j'} \quad \forall j' \in \{1, 2, \dots, J\} \setminus j \\ 0, & \text{otherwise.} \end{cases} \quad (37)$$

In practice, all the deployed UAVB-NIBs broadcast paging signals and the users can associate and connect to the one with the maximum received signal power [36].

C. Location Optimization

Consider the perfect CSI and RZF precoding to nullify co-channel interference between the users and decouple their information bearing signals. The UAVB-NIB localization problem is aimed at improving the channel gain between the UAVB-NIB and the associated users which will resultantly increase the SINR and AL rates in downlink communication scenario. The channel gain can be improved by adjusting the UAVB-NIB location parameters to enhance the scaling factors in (10) i.e., maximizing the antenna beam gain and minimizing FSPL. The higher antenna beam gain can be attained by using highly directional beams with concentrated radio frequency power, whereas, the FSPL can be decreased by adjusting UAVB-NIB altitude. Based on the derived J and α_k^j for a given beam coverage radius $r_j \forall j$, we now carry out the location parameter optimization i.e., $\mathbf{w}_j, r_j, H_j, \theta_j^{3\text{dB}}$, and $\phi_j^{3\text{dB}}$ for the worst-case scenario i.e., maximizing the minimum channel gain and minimizing the maximum path loss. Interestingly, these variable are related rendering only three independent variables $\mathbf{w}_j, r_j, \phi_j^{3\text{dB}}$ while other location parameters can be derived from these independent parameters using $\theta_j^{3\text{dB}} =$

$$\pi/2 - \phi_j^{3\text{dB}} \text{ and } H_j = r_j \tan(\phi_j^{3\text{dB}}).$$

$$\mathbf{P1(c)} : \text{maximize} \min_{\mathbf{w}_j, r_j, \phi_j^{3\text{dB}}} \alpha_k^j (G_{jk}^\Omega [\text{dB}] - L_{jk}^\Omega [\text{dB}]) \quad (38a)$$

$$\text{s.t.} \quad r_j \geq \max\{\alpha_k^j \|\mathbf{u}_k - \mathbf{w}_j\|\}, \forall k, j \quad (38b)$$

$$(31f), (31g), (31h), \text{ and } (32) \quad (38c)$$

The sub-problem **P1(c)** is disjoint problem for all j UAVB-NIBs and hence it can be solved independently for all UAVB-NIBs with the given set of associated users. The joint optimization of **P1(c1)** is difficult and complex owing to the non-convex nature due to the mixture of bessel functions, exponential functions, sinusoidal functions and multiple optimization parameters. Thus, it is hard to achieve a global optimal solution. However, decomposing this problem into sub-problems is a promising choice to obtain sub-optimal solution close to the optimal one. We can then employ block coordinate descent (BCD) method for alternate optimization of the parameters to successively maximize the objective functions along one coordinate while fixing the local values at the other coordinates in each iteration. This method guarantees local stationary point because objective function is monotonically increasing in each coordinate with every iteration i.e., $f(\mathbf{w}_j, r_j, \phi_j^{3\text{dB}}) \leq \max f(\mathbf{w}_j, r_j | \phi_j^{3\text{dB}}) \leq f(\mathbf{w}_j^*, r_j^*, \phi_j^{3\text{dB}}) \leq \max f(\phi_j^{3\text{dB}} | \mathbf{w}_j^*, r_j^*) \leq f(\mathbf{w}_j^*, r_j^*, \phi_j^{3\text{dB}*})$.

Considering the objective function $f(\mathbf{w}_j, r_j | \phi_j^{3\text{dB}})$ for j^{th} UAVB-NIB, the problem is equivalent to the minimum enclosing circle problem for a given set of points (users associated with j^{th} UAVB-NIB). Maximum sum rate can be achieved with maximum SNR by choosing minimum possible r_j to enclose all the points in a circle centered at \mathbf{w}_j . This will ensure highly directional beam and concentrated power to serve the given set of users. This can be reformulated as a quadratic programming problem in **P1(c1)**

$$\mathbf{P1(c1)} : \text{minimize}_{\kappa \in \mathbb{R}^{\varsigma_j}} \kappa^T \Xi_j \kappa - \mathbf{d}_j^T \kappa \quad (39a)$$

$$\text{s.t.} \quad \sum_{n=1}^{\varsigma_j} \kappa_n = 1, \quad \kappa_n \geq 0 \quad \forall n \quad (39b)$$

where $\Xi_j = \mathbf{U}_j \mathbf{U}_j^T$ and $\mathbf{d}_j = \text{diag}(\Xi_j)$ with $\mathbf{U} = [\mathbf{u}_1; \mathbf{u}_2; \dots; \mathbf{u}_K] \in \mathbb{R}^{K \times 2}$,

$$\mathbf{U}_j \in \mathbb{R}^{\varsigma_j \times 2}, \mathbf{U}_j \subseteq \mathbf{U}, \{\mathbf{u}_k \in \mathbf{U}_j | \alpha_k^j = 1\}.$$

Moreover, $\varsigma_j = \sum_{k=1}^K \alpha_k^j$ is the number of users associated with j^{th} UAVB-NIB. The Lagrange function of the revised problem **P1(c1)** can be written as:

$$\mathcal{L}(\iota, \kappa) = \kappa^T \Xi_j \kappa - \mathbf{d}_j^T \kappa - \iota \left(\sum_{n=1}^{\varsigma_j} \kappa_n = 1 \right); \iota \geq 0. \quad (40)$$

Solving this convex dual problem renders the primal and dual variables, which can then yield $\mathbf{w}_j^* = \mathbf{U}_j^T \kappa^*$ and $r_j^* = \sqrt{\kappa^{*T} \Xi_j \kappa^* - \iota^*}$. Based on the UAVB-NIB horizontal locations, we can now adjust individual altitudes using the optimal elevation angles $\phi_j^* \forall j$, by solving the following (see Appendix A) [37]

$$\frac{A}{1 + \bar{a} e^{-b \phi_{jk}^\Omega}} + 20 \log_{10}(r_j \sec \phi_{jk}^\Omega) + \bar{B}^\Omega = 0, \quad (41)$$

where $\bar{a} = a e^{ab}$. Interestingly, the evaluation of the optimal HPBW $\theta_j^{*3\text{dB}}$ and altitude H_j^* for each participating UAVB-NIB is a disjoint problem and can be solved independently.

Once the beamwidths are adjusted, the corresponding antenna beam gain for k^{th} user from the j^{th} UAVB-NIB can be evaluated using (12).

D. Resource Allocation

After UAV deployment, UA, and beam optimization, we focus on the design of power allocation parameters for the backhaul link. HAPS employs downlink NOMA strategy to simultaneously serve all the NIBs in its coverage area based on their locations and channel strength ordering. Thus, the power allocation problem for HAPS-NIB backhaul link can be written as:

$$\mathbf{P1(d)} : \underset{f_j}{\text{maximize}} \sum_{j=1}^J R_j(\Gamma_j) \quad (42a)$$

$$\text{s.t.} \quad R_{j \rightarrow l} \geq \tilde{R}_j, \forall j \leq l \quad (42b)$$

$$\sum_j f_j \leq 1, \quad \forall j \quad (42c)$$

$$0 \leq f_j \leq 1, \quad \forall j \quad (42d)$$

$$f_1 \geq f_2 \geq \dots \geq f_J \quad (42e)$$

Given the UAVB-NIB ordering $N_1 \leq N_2 \leq \dots \leq N_J$ with respect to their channel strengths, the target threshold constraint $R_{j \rightarrow l} \geq \tilde{R}_j, \forall j \leq l$ is most difficult to meet in the worst case scenario i.e., $j = l$. Thus, focusing on the worst case scenario, the constraint (42b) can be simplified as $R_j \geq \tilde{R}_j, \forall j$. Moreover, considering the same target threshold for all NIBs i.e., $\tilde{R}_j = R_{\text{th}}$, we can present the closed-form solution to this problem as [38]:

For the given UAVB-NIBs, there exists a UAVB-NIB j in $1 \leq j \leq J$, which satisfies the following condition:

$$\begin{cases} (2^{R_{\text{th}}/B_H} - 1) \left(\sum_{i=j}^J \aleph_i 2^{(i-1)R_{\text{th}}/B_H} \right) \leq 1, \\ (2^{R_{\text{th}}/B_H} - 1) \left(\sum_{i=j-1}^J \aleph_i 2^{(i-1)R_{\text{th}}/B_H} \right) \geq 1. \end{cases} \quad (43)$$

which indicates that the NIBs j to J can achieve the target rate threshold R_{th} owing to the better channel conditions, whereas, the NIB $j-1$ and weaker NIBs are unable to achieve the minimum threshold with the given power budget. Thus, we allocate the remaining power to the strongest NIB in order to maximize the sum data rate. Hence, the maximum achievable sum rate R_b^* , the power coefficients of NIBs f_j and the remaining power fraction Δf are given by

$$R_b^* = (J - j) R_{\text{th}} + B_H \log_2 \left[1 + \frac{\Delta f}{1 - \Delta f + \aleph_j} \right], \quad (44)$$

$$\hat{f}_j = \left(2^{R_{\text{th}}/B_H} - 1 \right) \left(\sum_{k=j+1}^J \hat{f}_k + \aleph_j \right), \quad (45)$$

$$\Delta f = 1 - \left(2^{R_{\text{th}}/B_H} - 1 \right) \left(\sum_{i=j}^J \aleph_i 2^{(i-1)R_{\text{th}}/B_H} \right). \quad (46)$$

The optimal sum rate in (44) comprises of two terms; the first term is the target rate threshold of NIBs j to J , whereas the second term is the additional rate of NIB J using the leftover power Δf . This indicates that NIBs j to J can attain target rates with assigned power coefficients $\hat{f}_j, \hat{f}_{j+1}, \dots, \hat{f}_J$ using (45). The remaining power with power allocation coefficient

Δf is insufficient for any of the remaining NIBs 1 to $j-1$ to fulfill their target threshold rate. Therefore, Δf in (46) is assigned to the strongest NIB J in order to maximize the overall sum rate.

Next is the resource allocation for the AL. The sum rate of the AL in scenarios III and IV is upper bounded by the rate of the backhaul link (44) derived by solving problem **P1(d)**. This subproblem is enumerated in problem **P1(e)**:

$$\mathbf{P1(e)} : \underset{p_{kj}^\Omega \forall k}{\text{maximize}} \sum_{j=1}^J \sum_{k=1}^K \sum_{\Omega} B_j^\Omega \log_2(1 + \gamma_{kj}^\Omega) \quad (47a)$$

$$\text{s.t.} \quad \tilde{R}_a(\gamma_{kj}^\Omega) \leq R_b^*, \quad \forall k \in K_1, j, \Omega \quad (47b)$$

$$R_{kj}^\Omega \geq R_{\text{min}}, \quad \forall k, j, \Omega \quad (47c)$$

$$\sum_k \sum_{\Omega} \alpha_k^j \beta_k^\Omega p_{kj}^\Omega \leq 1, \quad \forall j \quad (47d)$$

$$0 \leq p_{kj}^\Omega \leq 1, \quad \forall k, j, \Omega \quad (47e)$$

where $\tilde{R}_a(\gamma_{kj}^\Omega)$ is the subset of the AL rate comprising of the data rates of the set of users $k \in K_1$ in scenarios III and IV, which utilize the backhaul link for end-to-end communications. Assuming perfect RZF, we get $|\mathbf{h}_{kj}^{\Omega H} \mathbf{w}_{lj}^\Omega|^2 = 0, \forall k \neq l$. Thus, using (4), the objective function reduces to

$$R_a(p_{kj}^\Omega) = \sum_{j=1}^J \sum_{k=1}^K \sum_{\Omega} B_j^\Omega \log_2 \left(1 + \bar{\gamma}_{kj}^\Omega |\mathbf{h}_{kj}^{\Omega H} \mathbf{w}_{kj}^\Omega|^2 \alpha_k^j \beta_k^\Omega p_{kj}^\Omega \right). \quad (48)$$

The simplified expression shows an ideal concave objective function as the weighted sum of the logarithmic functions and convex constraints without (47b). For this non-convex constraint (47b), we propose to employ successive convex approximation (SCA) and find the convex approximation \tilde{R}_a and solve this problem iteratively. The first-order Taylor series approximation⁴ \tilde{R}_a around the power coefficient variables is given by:

$$\tilde{R}_a(\mathbf{p}, \mathbf{p}^{(i)}) \approx \tilde{R}_a(\mathbf{p}^{(i)}) + \nabla_{\mathbf{p}} \tilde{R}_a(\mathbf{p}^{(i)})^T (\mathbf{p} - \mathbf{p}^{(i)}), \quad (50)$$

where, \mathbf{p} is the vector comprising of the power coefficients of all users depending on their UAB-NIB association and demanded RAT and $\mathbf{p}^{(i)}$ is the chosen/updated power coefficients vector at instant (i) . The gradient $\nabla_{\mathbf{p}} \tilde{R}_a$ can be evaluated using the following partial derivatives:

$$\nabla_{\mathbf{p}} \tilde{R}_a = \begin{bmatrix} \alpha_1^j \beta_1^\Omega \frac{\partial \tilde{R}_a}{\partial p_{1j}^\Omega} & \alpha_2^j \beta_2^\Omega \frac{\partial \tilde{R}_a}{\partial p_{2j}^\Omega} & \dots & \alpha_K^j \beta_K^\Omega \frac{\partial \tilde{R}_a}{\partial p_{Kj}^\Omega} \end{bmatrix}, \quad (51)$$

where

$$\frac{\partial \tilde{R}_a}{\partial p_{kj}^\Omega} = \sum_j \sum_{\bar{k}} \sum_{\Omega} \frac{B_j^\Omega}{\log(2)} \frac{\bar{\gamma}_{kj}^\Omega |\mathbf{h}_{kj}^{\Omega H} \mathbf{w}_{kj}^\Omega|^2 \alpha_k^j \beta_k^\Omega}{1 + \bar{\gamma}_{kj}^\Omega |\mathbf{h}_{kj}^{\Omega H} \mathbf{w}_{kj}^\Omega|^2 \alpha_k^j \beta_k^\Omega p_{kj}^\Omega}. \quad (52)$$

It is interesting to note that the gradient $\nabla_{p_{kj}^\Omega} \tilde{R}_a$ can be conveniently computed owing to the disjoint data rate of each user as a function of the allocated power fraction. This leads to the convex approximation of the constraint (47b). Thus, problem **P1(e)** can be iteratively solved using the successive convex approximation method. The non-convex mixed integer programming problem **P1** can be solved using the convexifica-

⁴ First order Taylor series expansion of a function $f(x)$ around a point $x^{(k)}$ is given as

$$\tilde{f}(x, x^{(k)}) \approx f(x^{(k)}) + \nabla_x f(x^{(k)}) (x - x^{(k)}). \quad (49)$$

Algorithm 1 Sequential Optimization Algorithm

- 1: **Input:** The number $\{K\}$, the coordinates of users $\{\mathbf{u}_k\}$ in the horizontal plane, radius of desired coverage area $\{R\}$, UAVB-NIB operable RATs Ω , users RAT preference β_k^Ω , NIB transmission power for each RAT $P_j^\Omega \forall \Omega$, HAPS transmission power P_H , UAVB-NIBs transmission power P_j^Ω and station-keeping altitude $\{H\}$.
 - 2: **Initialize** $i \leftarrow 0$, $R_a[i-1] \leftarrow R_0$ and $\epsilon \leftarrow \infty$
 - 3: **Select** QoS minimum rate threshold R_{\min} , minimum possible beam radius r_{\min} , and regularization scalar ω
 - 4: **Set** tolerance δ , $r[i] = r_{\min}$, and $r_{\text{UB}} = R$
 - 5: **Choose** Δr and identical beam radius $r_j[i] = r[i] \forall m$
 - 6: **while** $\epsilon \geq \delta$ & $r_{\min} \leq r_j[i] \leq R$ **do**
 - 7: **Let** $i \leftarrow i + 1$
 - 8: **Update** $r_j[i] = r_j[i-1] + \Delta r$ for all UAVB-NIBs ensuring sequential increment with every iteration.
 - 9: **Determine** $M[i]$ and $\mathbf{w}_j[i] \forall m \in [1, M]$ using GDC to solve **P1(a)** in (34) given constant $r[i]$.
 - 10: **Associate** users by solving **P1(b)** in (36) to evaluate $\alpha_k^j[i]$ using greedy algorithm.
 - 11: **Optimize** individual UAVB-NIB to evaluate beam parameters $\tilde{w}_j[i]$, $\tilde{\theta}_j[i]$ and $\tilde{r}_j[i]$ by solving **P1(c)** in (39).
 - 12: **Update** $w_j[i] \leftarrow \tilde{w}_j[i]$, $r_j[i] \leftarrow \tilde{r}_j[i]$ and $\theta_j[i] \leftarrow \tilde{\theta}_j[i]$.
 - 13: **Obtain** the available transmit power $P_H[i]$ of a solar powered HAPS at the chosen location on a given date and time of the day using the power estimation algorithms [26].
 - 14: **Calculate** the channel coefficients $g_j[i]$ and $h_{kj}^\Omega[i]$ using the pathlosses $L_j^{\text{HAPS}}[i]$ and beam gain $G_j^{\text{HAPS}}[i] \forall j$ for the backhaul and pathloss $L_{jk}^\Omega[i]$ and beam gain $G_{jk}^\Omega[i] \forall j, k, \Omega$ for the AL, respectively.
 - 15: **Compute** the power allocation coefficients $f_j[i]$ for each UAVB-NIB using the closed form solutions of **P1(d)** in (42) for the given QoS threshold \tilde{R}_j and NIB ordering.
 - 16: **Compute** the power allocation coefficients $p_{kj}^\Omega[i]$ for each user by solving **P1(e)** in (47).
 - 17: **Evaluate** the sum rate in the AL $R_a[i]$ and backhaul sum rate $R_b[i]$
 - 18: **Compare** $R_a[i]$ with $R_a[i-1]$
 - 19: if $R_a[i] \geq R_a[i-1]$: $R_a^*[i] \leftarrow R_a[i]$
 - 20: if $R_a[i] \leq R_a[i-1]$: $R_a^*[i] \leftarrow R_a[i-1]$
 - 21: Update $\epsilon \leftarrow R_a[i] - R_a[i-1]$
 - 22: **end while**
 - 23: User grouping parameters: $J^* \leftarrow J[i]$, $\mathbf{w}_j^* \leftarrow \mathbf{w}_j[i]$
 - 24: UA parameters: $\alpha_k^{j*} \leftarrow \alpha_k^j[i] \forall l, m$
 - 25: Beam radii: $r_j^* \leftarrow r_j[i]$
 - 26: Half-power beam widths: $\theta_j^* \leftarrow \theta_j[i] \forall m$
 - 27: Backhaul power allocation parameters: $f_j^* \leftarrow f_j[i] \forall j$
 - 28: AL power allocation parameters: $p_{kj}^{\Omega*} \leftarrow p_{kj}^\Omega[i] \forall k, j, \Omega$
 - 29: Sum rate of GUs: $R_a^* \leftarrow R_a[i]$
-

tion of each individual sub-problem. Each sub-problem is then independently solved for fewer variables, assuming the rest as given constants, as detailed in Algorithm 1. Although the sub-problems are solved independently, however, the presented sequential order is crucial. It is pivotal to evaluate the serving

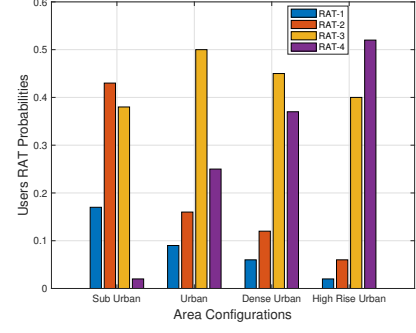


Fig. 4: Users RAT Probabilities ($P_{r\Omega}$)

number and locations of UAVB-NIB before user association. Deployment enables users to associate with the nearest UAVB-NIB rendering maximum signal strength. Likewise, UA helps in location optimization to form directive beams. Eventually, deployment and association permits the optimal resource allocation from the identified UAVB-NIB to the group of associated users demanding particular RATs.

VI. NUMERICAL RESULTS AND DISCUSSION

We adopt PHASA-35 HAPS aircraft model flying at an altitude of 20km and evaluate the available transmit power for noon on the winter and summer solstice of 2025 using the solar algorithms [26]. The analysis assumes different areas; sub urban, urban, urban, dense urban, and high rise urban with different user densities, where users are distributed as Poisson Point Process. In addition, each UAVB-NIB is capable of offering 4 RAT technologies to the GUs with different probabilities according to the user population, as illustrated in Fig. 4. We assume distinct carrier frequencies and appropriate bandwidths for each RAT technology. We aim to carry out a thorough numerical analysis to quantify the gains achieved by each step in the proposed heterogeneous communication system.

A. Illustration of the Proposed Sequential Algorithm

The sequential optimization of the proposed UAVB-NIB deployment, UA, and location optimization is illustrated in Fig. 5. Color-coded users operating at different RATs and distributed as Poisson point process in the circular HAPS coverage area of 150km radius are demonstrated in Fig. 5(a). RAT-1 (yellow) is the least probable whereas RAT-4 (blue) is the preferred access technology for the GUs in this configuration area using the probabilities in Fig. 4. Next, we determine the initial coverage zones for UAVB-NIB deployment using the GDC algorithm, which render 24 required UAVB-NIBs and their central locations for a given beam radius as depicted in Fig. 5(b). It is followed by the UA using greedy algorithm where the users associate themselves with the UAVB-NIB based on the maximum received SINR. Fig. 5(c) presents the UA using green lines merging towards the beam center marked by the UAVB-NIB's projection on ground. This UA allows us to concentrate the antenna beams towards the active users while optimizing the beams parameters and UAVB-NIBs locations. Fig. 5(d) exhibits the optimal UAVB-NIB locations and reduced coverage/beam radii to serve the predefined associated users. Clearly, this minimizes the overlapping regions and maximizes the power density in a given beam which increases

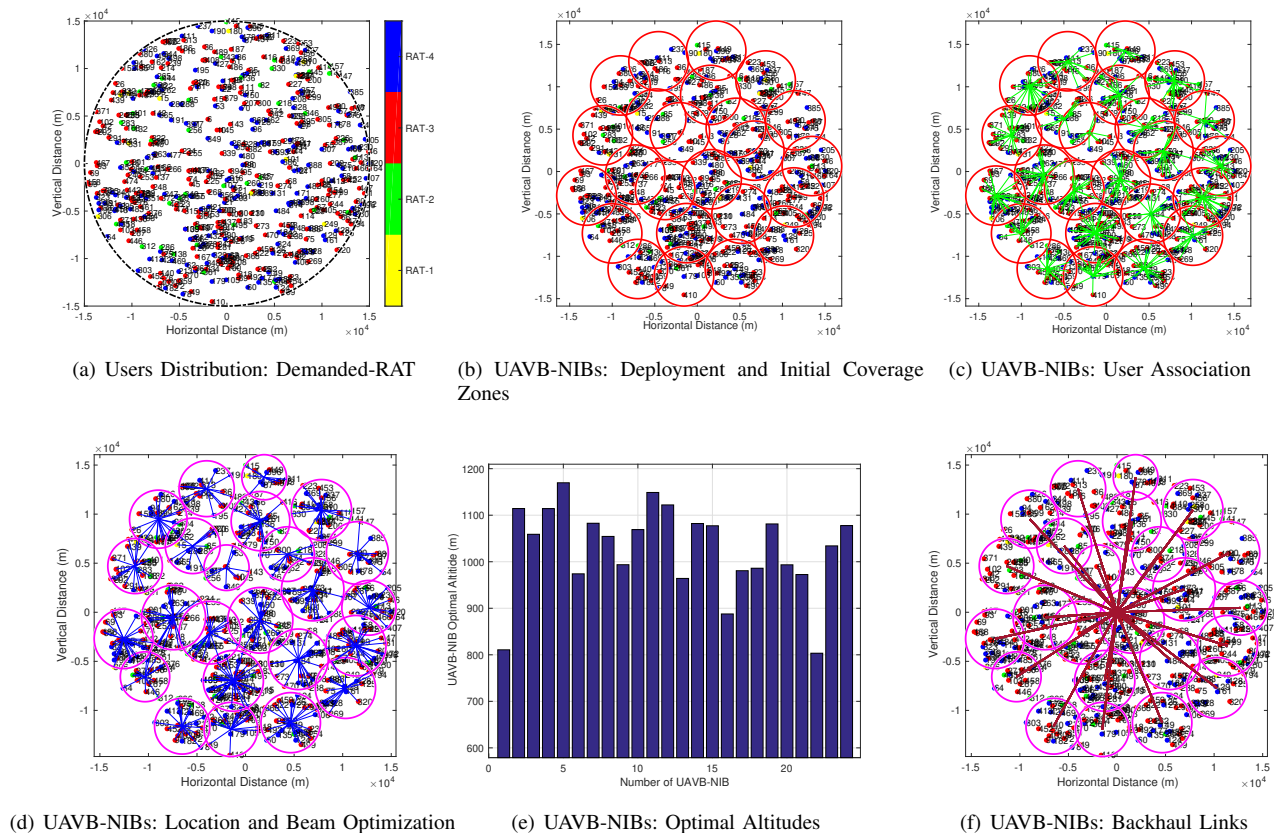


Fig. 5: UAVB-NIBs deployment, user association and parameters optimization

the SINR and consequently the sum-rate of the users. On the other hand, optimal flying altitudes of the 24 participating UAVB-NIBs are highlighted in Fig. 5(e). Eventually, Fig. 5(f) displays the backhaul connection of each UAVB-NIB with the HAPS positioned at the origin without loss of generality. Fig. 5 displays the step-by-step approach to tackle the UAVB-NIB deployment and UA problems. These optimized parameters can then be utilized for optimal resource allocation by UAVB-NIBs and HAPS in the access and backhaul downlink, respectively.

B. UAVB-NIB Deployment Schemes

In order to validate the effectiveness of UAVB-NIB deployment algorithm, we study the minimum number of required UAVB-NIBs in a sub-urban area with user density 1000 users/km² and radius ranging from 5km to 17km. We assume two different antenna beam sizes for the participating UAVB-NIBs termed as small and large beam-radii with values 2.5km and 3.5km, respectively. Evidently, the number of required UAVB-NIBs increases with the increasing coverage radius and consequently increasing number of GUs in that area as detailed in Fig. 6(a). Intuitively, a large number of narrow-beamed UAVB-NIBs are required to serve a certain coverage area as compared to the wide-beamed UAVB-NIBs. Interestingly, the proposed UAVB-NIB deployment GDC scheme renders significantly less number of required UAVB-NIBs as opposed to the conventional deployment. The step-wise increase in

the conventional cellular deployment is owing to the increase in tier of UAVs for a certain change in coverage radius which then stays the same for a range of coverage radii before adding another tier/layer of UAVs. At around 16km coverage radius the difference between proposed GDC and conventional approach is around 35 narrow-beamed UAVB-NIBs as opposed to 62 narrow-beamed UAVB-NIBs and 23 wide-beamed UAVB-NIBs relative to the 38 wide-beamed UAVB-NIBs, respectively. We can conclude that the proposed users-aware deployment scheme can serve a given coverage area with up to 50% less UAVB-NIBs than the conventional deployment.

C. Performance of Different UA Strategies

We evaluate the performance of the proposed SNR-based UA (UA-SNR) algorithm with distance-based UA algorithm (UA-DB) and random UA (UA-Rand) in Fig. 6(b). We investigate the average received SINR at the GUs in the same sub urban setting with narrow-beamed and wide-beamed UAVB-NIBs. For a given user distribution, we evaluate the optimal number and locations of the UAVB-NIBs. Then, we perform user-association with pre-defined UAVB-NIBs locations using the three aforementioned UA algorithms to study the average received SINR of the GUs. Expectedly, the average received SINR increases with the increased transmission power and especially for the narrow-beamed UAVB-NIBs. Interestingly, the UA-DB performs equally well as the proposed UA-SNR

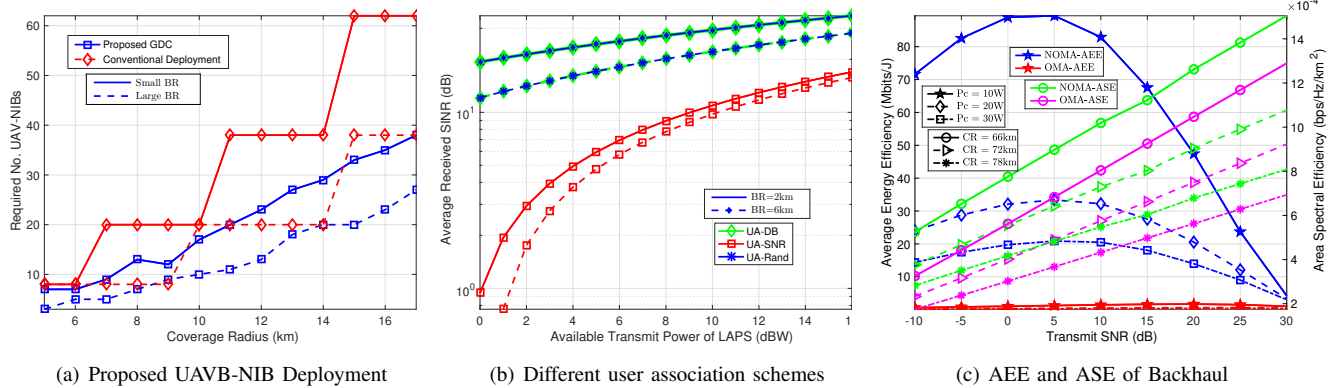


Fig. 6: Parameters optimization and resource allocation

whereas UA-Rand demonstrates degraded performance for the entire range of transmission power. Using 10dBW transmission power of each participating UAVb-NIB, we observe almost 20dB difference in the average received SINR of the GUs signifying the importance of the appropriate UA instead of random user association.

D. Energy and Spectral Efficiency of the Backhaul

Aerial communications are predominantly restricted by the available power budget [26]. This manifests energy efficiency⁵ as a critical performance metric for the solar-powered HAPS. Energy efficient communication with cognizant power control can significantly impact and prolong the flight operation times. We can compute the average energy efficiency (AEE) of the backhaul link AEE_b using

$$AEE_b = \frac{1}{J} \sum_{j=1}^J \frac{R_j}{f_j P_H + P_{c_2}}, \quad (53)$$

where R_j is the achievable rate of j^{th} UAVB-NIB with power allocation $f_j P_H$ and circuit power consumption of P_{c_2} in the backhaul. Similarly, the spectrum efficiency⁶ describes the amount of data transmitted over a given spectrum with minimum transmission errors. The average SE of the backhaul link with NOMA can be viewed as $SE_{\text{avg}}^b = \frac{1}{J} \sum_j R_j / B_H$, while the area SE (ASE) of the backhaul link can be presented as:

$$ASE_b = \frac{SE_{\text{avg}}^b}{\pi R^2}, \quad (54)$$

The described AEE and ASE of the backhaul link between HAPS and UAVB-NIBs are analyzed for optimal versus sub-optimal resource allocation strategies in Fig. 6(c). We assume an urban area of 60km radius and 3000users/km² user density served by the wide-beamed UAVB-NIBs with beam radii 5km. We further assume 6.4GHz carrier frequency with 100MHz channel bandwidth for the backhaul connection. The AEE is observed for the range of transmit SNR for three different circuit power consumption scenarios i.e., $P_c = 10\text{W}$, $P_c = 20\text{W}$, and $P_c = 30\text{W}$. Evidently, the AEE of NOMA based

power allocation outperforms the OFDMA counterpart for the entire range of transmit SNR. Moreover, the NOMA-AEE decreases with increasing circuit power consumption whereas the NOMA-AEE initially increases with increasing transmit SNR and then decreases with further increase in transmit SNR. This renders the maximum NOMA-AEE of 90Mbits/J around 5dB transmit SNR for all circuit power consumptions. In addition, the Fig. 6(c) reveals the ASE of the same system for three different coverage radii. Clearly, the ASE decreases with increasing coverage area as the same HAPS resources are now utilized to serve increasing number of users requiring more UAVB-NIBs with fixed beam coverage areas. Moreover, the SE increases with the increasing transmit SNR owing to the increase in the achievable rate. Lastly, the NOMA-ASE outperforms OMA-ASE for all transmit SNR and all coverage radii. For instance, NOMA-ASE renders around 20% percentage increase over conventional OMA-ASE at 20dB transmit SNR.

E. Average Sum Rate Performance

The impact of the proposed non-uniform power allocation (NUPA) strategy is compared with the conventional uniform power allocation (UPA) on the average sum rate of the AL. Fig. 7(a) presents the downlink sum rate with the UAVB-NIB transmission power budget ranging from 0dBW to 16dBW for three different area configurations. Sub urban, urban, and dense urban areas are assumed to have distinct user densities i.e., 1000users/km², 3000users/km², and 5000users/km², respectively. In addition, they have unique environmental parameter pairs $(\eta_{\text{LOS}}, \eta_{\text{NLOS}})$; (0.1, 21), (1.0, 20), and (1.6, 23) in respective order [39]. The values of the constants are $a = 11.95$, and $b = 0.136$ [40] whereas the RAT operational demands according to the area configurations are shown in Fig. 4. We suppose maximum antenna gain of UAVB-NIBs $G_{\text{max}} = 23\text{dBi}$, HPBW $\theta_j^{3\text{dB}} = 12^\circ$ and transmit diversity $M = 2$, unless specified otherwise. The sum rates of LAPS-GUs downlink are averaged over numerous channel instances. Evidently, the sum rate increases with the increase in transmission power, however, the gain is particularly significant in optimal power allocation strategy. We further observe that dense urban area exhibits highest sum rates owing to the

⁵EE is measured in bits/Joules i.e., a higher value of EE indicates the higher amount of data in bits that can be sent with minimal energy consumption.

⁶It is a measure of how efficiently a limited frequency spectrum is utilized to transmit the data by the proposed communication system. It is typically measured in bps/Hz.

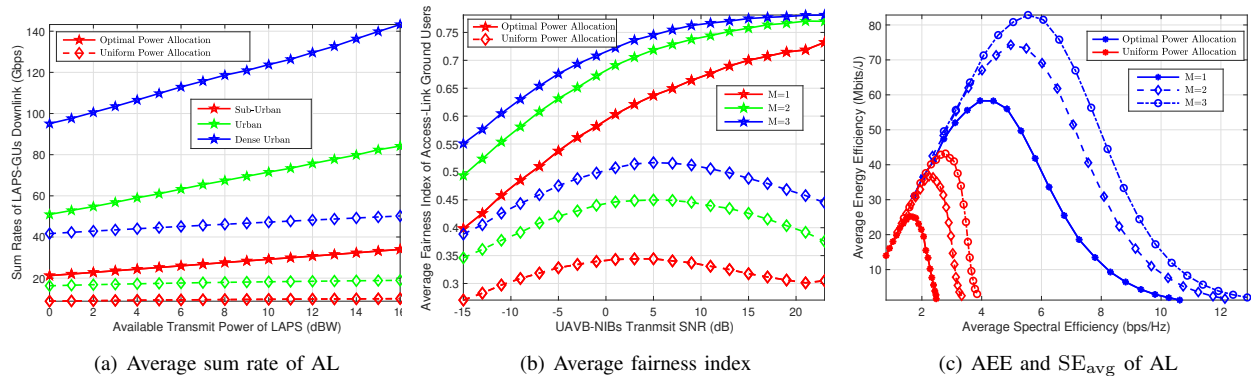


Fig. 7: Effect of optimal resource allocation on sum-rate, fairness index, EE and SE in the AL

high user-density requiring concentrated beams from a large number of UAVB-NIBs to serve the given coverage area. We can observe the percentage increase in average sum rate upto 185.24% with the proposed optimal power allocation over the uniform power assignment.

F. Jain's fairness index

The fairness of a communication system is analyzed to determine whether all participating nodes are receiving a fair share of the system resources. The UF of the GUs in the AL can be quantified using the Jain's fairness index as:

$$\mathcal{J}_a = \frac{(\sum_{k=1}^K R_{kj}^\Omega)^2}{K \cdot \sum_{k=1}^K R_{kj}^\Omega}. \quad (55)$$

The UF is evaluated for a dense urban area versus transmit SNR for varying number of transmit antennas in Fig. 7(b). The average fairness index (AFI) is the fairness index of all users in the given coverage area averaged over numerous channel instances. Intriguingly, the AFI increases with increasing transmit diversity and optimal power allocation clearly renders higher AFI than the uniform counterpart. Interestingly, we observe different trends of the two power allocation schemes with respect to the transmit SNR. Increasing transmit SNR results in increasing fairness amongst users for the NUPA. However, it initially increases and then decreases with increasing transmit SNR for the UPA. The UPA yields maximum AFI at 5dB SNR but this is still 30% less than the AFI of optimal power allocation at same SNR. We observe 85%, 59.75%, and 44.28% percent improvement in AFI using the proposed power allocation over uniform power allocation with $M = 1, 2,$ and 3 transmit antennas, respectively.

G. System Efficiency of the AL

The system efficiency of the AL can also be evaluated in terms of AEE and ASE. The EE metric is specifically beneficial for UAVB-NIBs operating in remote or hard-to-access areas where battery replacement or recharging may be challenging. In the AL, the AEE of the AL can be seen as the averaged EE of all the users under UAVB-NIBs coverage i.e.,

$$\text{AEE}_a = \frac{1}{K} \sum_{j=1}^J \sum_k \sum_\Omega \frac{R_{kj}^\Omega}{p_{kj}^\Omega P_j^\Omega + P_{c1}} \quad \forall k, \quad (56)$$

where R_{kj}^Ω and p_{kj}^Ω are the achievable rate and power allocation factors of the concerned user in the respective order, P_j and P_{c1} are the power budget and circuit power expenditures, respectively. Moreover, assuming the perfect CSI and RZF, we can write the average SE of the AL as:

$$\text{SE}_{\text{avg}}^a = \frac{1}{K} \sum_j \sum_k \sum_\Omega R_{kj}^\Omega / B_j^\Omega \quad (57)$$

The overall SE is averaged for all RATs as each one offers its own bandwidth to the operational set of users. The AEE versus SE_{avg}^a of the AL is evaluated for the same system parameters. The AEE appears to be a concave function of SE_{avg}^a rendering maximum value of 82.84Mbits/J at 5bps/Hz for optimal power allocation as opposed to the maximum value of 43.2Mbits/J at 3bps/Hz for UPA. Fig. 7 demonstrates the concentrated values on the lower-left bottom of the graph for UPA as compared to the right-top values for optimal power allocation. This signifies the lower AEE and SE_{avg}^a values of UPA versus higher AEE and SE_{avg}^a values of optimal power allocation for any number of transmit antennas. We can quantify the percentage improvement in the peak AEE values with optimal power allocation over the UPA as 132.52%, 104.2%, and 91.77% for $M = 1, 2,$ and 3 transmitting UAVB-NIB antennas, respectively.

VII. CONCLUSIONS

The compact, portable, and versatile NIB solution along with heterogeneous aerial communication platforms i.e., LAPS and HAPS can formulate an intelligent aerial wireless network for remote coverage. Such combination for the access and backhaul link offers flexible, scalable, and resilient coverage solution. We have proposed NOMA for the backhaul connection between HAPS and UAVB-NIBs whereas zero-forcing scheme for the access MISO downlink channel between UAVB-NIBs and GUs. In addition, we have presented geometric disk cover for optimal UAVB-NIB deployment, greedy algorithm for user association, Lagrange optimization for the location optimization and successive convex approximation for the resource allocation problem in order to improve the system performance. The proposed algorithms and design guidelines enable this intelligent network to configure, deploy, and serve with the effective resource allocation, minimal power consumption, and enhanced system performance at the desired

coverage area as per the users demand and QoS thresholds. Numerical results have revealed up to 50% less number of required UAVB-NIBs, 20% improvement in backhaul ASE, 185.24% increase in the average sum rate of the AL, and 85% improvement in average UF with the proposed strategies.

VIII. ACKNOWLEDGMENT

This work is supported in part by the King Abdullah University of Science and Technology Research Funding (KRF) under Award ORA-2021-CRG10-4696. The work of Yunfei Chen is also supported by EPSRC TITAN (EP/Y037243/1, EP/X04047X/1). The work of Cheng-Xiang Wang is also supported by the National Natural Science Foundation of China (NSFC) under Grant 61960206006 and the EU H2020 RISE TESTBED2 project under Grant 872172.

APPENDIX A OPTIMAL ELEVATION ANGLE

We can write the path loss of the AL between k^{th} user and j^{th} UAVB-NIB operation at Ω RAT as a function of the elevation angle ϕ_{jk}^{Ω} as:

$$L_{jk}^{\Omega}[\text{dB}] = \frac{A}{1 + \bar{a}e^{-b\phi_{jk}^{\Omega}}} + 20 \log_{10}(r_j \sec \phi_{jk}^{\Omega}) + \bar{B}^{\Omega} \quad (58)$$

where $\bar{a} = ae^{ab}$ and

$$\bar{B}^{\Omega} = 20 \log_{10} \left(\frac{4\pi f_c^{\Omega}}{c} \right) + \eta_{\text{NLOS}} \quad (59)$$

Interestingly, for the worst case scenario $\phi_{jk}^{\Omega} = \phi_j$ i.e., path loss is maximum at the cell edge. Thus, solving $\mathbf{P1(c)}$ is equivalent to minimizing $L_{jk}^{\Omega}[\text{dB}]$ with respect to ϕ_j for the given r_j^* and \mathbf{w}_j^* . It is straight forward to prove that the path loss in (58) is convex in ϕ_j by showing that $\frac{\partial^2 L_{jk}^{\Omega}}{\partial \phi_j^2} \geq 0$. Hence, the first-order stationary point is the optimal ϕ_j^* , which can be attained by solving $\frac{\partial L_{jk}^{\Omega}}{\partial \phi_j} = 0$.

REFERENCES

- [1] M. Matracia, A. U. Rahman, R. Wang, M. A. Kishk, and M.-S. Alouini, "Bridging the digital divide," in *Fundam. of 6G Commun. and Netw.* Springer, 2023, pp. 113–139.
- [2] W. Xu, Y. Huang, W. Wang, F. Zhu, and X. Ji, "Toward ubiquitous and intelligent 6G networks: from architecture to technology," *Sci. China Inf. Sci.*, vol. 66, no. 3, p. 130300, 2023.
- [3] C.-X. Wang, Z. Lv, Y. Chen, and H. Haas, "A complete study of space-time-frequency statistical properties of the 6G pervasive channel model," *IEEE Trans. Commun.*, 2023.
- [4] S. Chandrasekharan, K. Gomez, A. Al-Hourani, S. Kandeepan, T. Rasheed, L. Goratti, L. Reynaud, D. Grace, I. Bucaille, T. Wirth *et al.*, "Designing and implementing future aerial communication networks," *IEEE Commun. Mag.*, vol. 54, no. 5, pp. 26–34, 2016.
- [5] C.-X. Wang, X. You, X. Gao, X. Zhu, Z. Li, C. Zhang, H. Wang, Y. Huang, Y. Chen, H. Haas *et al.*, "On the road to 6G: Visions, requirements, key technologies and testbeds," *IEEE Commun. Surveys Tuts.*, 2023.
- [6] T. Zhang, C. Chen, Y. Xu, J. Loo, and W. Xu, "Joint task scheduling and multi-uav deployment for aerial computing in emergency communication networks," *Sci. China Inf. Sci.*, vol. 66, no. 9, p. 192303, 2023.
- [7] H. Chang, C.-X. Wang, J. Bian, R. Feng, Y. He, Y. Chen, and E.-H. M. Aggoune, "A novel 3D beam domain channel model for UAV massive MIMO communications," *IEEE Trans. Wireless Commun.*, 2023.
- [8] M. Benzaghta, G. Geraci, R. Nikbakht, and D. López-Pérez, "UAV communications in integrated terrestrial and non-terrestrial networks," in *IEEE Global Commun. Conf. (GLOBECOM)*, Rio de Janeiro, Brazil, Dec. 2022, pp. 3706–3711.
- [9] B. E. Y. Belmekki, A. J. Aljohani, S. A. Althubaity, A. Al Harthi, K. Bean, A. Aijaz, and M.-S. Alouini, "Cellular network from the sky: Toward people-centered smart communities," *IEEE Open J. Commun. Soc. (OJ-COMS)*, 2024.
- [10] M. Pozza, A. Rao, H. Flinck, and S. Tarkoma, "Network-in-a-box: A survey about on-demand flexible networks," *IEEE Commun. Surveys Tuts.*, vol. 20, no. 3, pp. 2407–2428, 2018.
- [11] C.-H. Hsu, G. Manogaran, G. Srivastava, and N. Chilamkurti, "Guest editorial: 6G-enabled network in box (NIB) for industrial applications and services," *IEEE Trans. Ind. Informat.*, vol. 17, no. 10, pp. 7141–7144, 2021.
- [12] A. Anjum, "Securitisation of cyber space-from prism of deterrence strategy," *Authorea Preprints*, 2023.
- [13] R. J. Sánchez, J. B. Evans, G. J. Minden, V. S. Frost, and K. S. Shanmugan, "RDRN: a rapidly deployable radio network-implementation and experience," in *IEEE Int. Conf. on Univ. Pers. Commun. Conf. Proc. (ICUPC'98)*, vol. 1, Florence, Italy, Oct. 1998, pp. 93–97.
- [14] J. B. Evans, G. J. Minden, K. S. Shanmugan, G. Prescott, V. S. Frost, B. Ewy, R. Sanchez, C. Sparks, K. Malinimohan, J. Roberts *et al.*, "The rapidly deployable radio network," *IEEE J. Sel. Areas Commun.*, vol. 17, no. 4, pp. 689–703, 1999.
- [15] J.-S. Huang, Y.-N. Lien, and C.-L. Hu, "Design of contingency cellular network," in *14th IEEE Asia-Pacific Netw. Op. Manag. Symp. (APNOMS)*, Seoul, Sep. 2012, pp. 1–4.
- [16] K.-H. Park, M.-S. Alouini, and Y. Chen, "Network-in-a-box to provide health services in remote areas," *ITU Connect2Recover Initiative*, 2022.
- [17] G. Sun, Z. Xu, H. Yu, and V. Chang, "Dynamic network function provisioning to enable network in box for industrial applications," *IEEE Trans. Ind. Informat.*, vol. 17, no. 10, pp. 7155–7164, 2020.
- [18] Z. Lv, L. Qiao, and I. You, "6G-enabled network in box for internet of connected vehicles," *IEEE Trans. Intell. Transp. Syst.*, vol. 22, no. 8, pp. 5275–5282, 2020.
- [19] J. Zhang, Z. Wang, D. Wang, X. Zhang, B. B. Gupta, X. Liu, and J. Ma, "A secure decentralized spatial crowdsourcing scheme for 6G-enabled network in box," *IEEE Trans. Ind. Informat.*, vol. 18, no. 9, pp. 6160–6170, 2021.
- [20] D. Iland and E. M. Belding, "EmergeNet: Robust, rapidly deployable cellular networks," *IEEE Commun. Mag.*, vol. 52, no. 12, pp. 74–80, 2014.
- [21] K. Heimerl, S. Hasan, K. Ali, E. Brewer, and T. Parikh, "Local, sustainable, small-scale cellular networks," in *6th Int. Conf. Inf. Commun. Tech. Dev.: Full Papers-Volume 1*, 2013, pp. 2–12.
- [22] F. Hsieh, F. Jardel, E. Visotsky, F. Vook, A. Ghosh, and B. Picha, "UAV-based multi-cell HAPS communication: System design and performance evaluation," in *Proc. Global Commun. Conf. (GLOBECOM)*. Taipei, Taiwan: IEEE, Dec. 2020, pp. 1–6.
- [23] C. B. Peel, B. M. Hochwald, and A. L. Swindlehurst, "A vector-perturbation technique for near-capacity multi-antenna multiuser communication-part i: channel inversion and regularization," *IEEE Trans. Commun.*, vol. 53, no. 1, pp. 195–202, 2005.
- [24] Y. Shibata, N. Kanazawa, M. Konishi, K. Hoshino, Y. Ohta, and A. Nagate, "System design of Gigabit HAPS mobile communications," *IEEE Access*, vol. 8, pp. 157995–158007, 2020.
- [25] Y. Ata and M.-S. Alouini, "HAPS based FSO links performance analysis and improvement with adaptive optics correction," *IEEE Trans. Wireless Commun.*, 2022.
- [26] S. Javed, M.-S. Alouini, and Z. Ding, "An interdisciplinary approach to optimal communication and flight operation of high-altitude long-endurance platforms," *IEEE Trans. Aerosp. Electron. Syst.*, 2023.
- [27] G. Zheng, S. Chatzinotas, and B. Ottersten, "Generic optimization of linear precoding in multibeam satellite systems," *IEEE Trans. Wireless Commun.*, vol. 11, no. 6, pp. 2308–2320, 2012.
- [28] Y. Wang, X. Fang, W. Feng, Y. Chen, N. Ge, and Z. Lu, "On-demand coverage for maritime hybrid satellite-uav-terrestrial networks," in *IEEE Int. Conf. Wirel. Commun. Signal Process. (WCSP)*, Nanjing, China, 2020, pp. 483–488.
- [29] F. Hsieh and M. Rybakowski, "Propagation model for high altitude platform systems based on ray tracing simulation," in *13th IEEE Eur. Conf. Antennas Propag. (EuCAP)*, Krakow, Poland, Apr. 2019, pp. 1–5.
- [30] J. L. Cuevas-Ruiz and J. A. Delgado-Penín, "Channel modeling and simulation in HAPS systems," *Eur. Wirel.*, pp. 24–27, 2004.
- [31] A. G. Kanatas and A. D. Panagopoulos, *Radio wave propagation and channel modeling for earth-space systems*. CRC Press, 2017.
- [32] A. A. O. OLADIPO, "Stratospheric propagation and HAPS channel modeling," *MS Thesis at Blekinge Institute of Tech., School of Eng., Department of Telecommun. Sys.*, 2007.
- [33] M. Takahashi, Y. Kawamoto, N. Kato, A. Miura, and M. Toyoshima, "Adaptive power resource allocation with multi-beam directivity control in high-throughput satellite communication systems," *IEEE Wireless Commun. Lett.*, vol. 8, no. 4, pp. 1248–1251, 2019.
- [34] A. S. Academy, "Space communication calculations," Jan. 2017.

- [35] B. Liu, C. Jiang, L. Kuang, and J. Lu, "Joint user grouping and beamwidth optimization for satellite multicast with phased array antennas," in *IEEE Global Commun. Conf. (GLOBECOM)*, Taipei, Taiwan, Dec. 2020, pp. 1–6.
- [36] A. Alkhateeb, Y.-H. Nam, M. S. Rahman, J. Zhang, and R. W. Heath, "Initial beam association in millimeter wave cellular systems: Analysis and design insights," *IEEE Trans. Wireless Commun.*, vol. 16, no. 5, pp. 2807–2821, 2017.
- [37] A. Al-Hourani, S. Kandeepan, and S. Lardner, "Optimal LAP altitude for maximum coverage," *IEEE Wireless Commun. Lett.*, vol. 3, no. 6, pp. 569–572, 2014.
- [38] K. Wang, Y. Liu, Z. Ding, A. Nallanathan, and M. Peng, "User association and power allocation for multi-cell non-orthogonal multiple access networks," *IEEE Trans. Wireless Commun.*, vol. 18, no. 11, pp. 5284–5298, Nov. 2019.
- [39] A. Al-Hourani, S. Kandeepan, and A. Jamalipour, "Modeling air-to-ground path loss for low altitude platforms in urban environments," in *IEEE Global Commun. Conf.*, Austin, TX, USA, Dec. 2014, pp. 2898–2904.
- [40] Y. Sun, Z. Ding, and X. Dai, "A user-centric cooperative scheme for UAV-assisted wireless networks in malfunction areas," *IEEE Trans. Commun.*, vol. 67, no. 12, pp. 8786–8800, 2019.